Phase Behaviors of Room Temperature Ionic Liquid Linked with Cation Conformational Changes: 1-Butyl-3-methylimidazolium Hexafluorophosphate

Takatsugu Endo,[†] Tatsuya Kato,[†] Ken-ichi Tozaki,[‡] and Keiko Nishikawa*[,†]

Graduate School of Advanced Integration Science, Chiba University, 1-33 Yayoi-cho, Inage-ku, Chiba 263-8522, Japan, and Faculty of Education, Chiba University, 1-33 Yayoi-cho, Inage-ku, Chiba 263-8522, Japan

Received: September 25, 2009; Revised Manuscript Received: October 27, 2009

We have investigated phase-transition behaviors of a typical room temperature ionic liquid, 1-butyl-3-methylimidazolium hexafluorophosphate ($[C_4mim]PF_6$), using calorimetric and Raman spectroscopic techniques. Although there was some confusion on its phase behaviors in previous reports, our measurements with a laboratory-made calorimeter at a slow scanning rate (5 mK/s) have definitely revealed that $[C_4mim]PF_6$ has three crystalline phases. From the Raman spectroscopic study, the conformations of the butyl group for these crystalline phases are assigned to gauche−trans, trans−trans, and gauche'−trans conformations in lower-energy order. It has been also shown that these three conformers coexist in the liquid, supercooled liquid, and glass states. It is concluded that all of the phase transitions of $[C_4mim]PF_6$ except the glass transition are associated with conformational changes of the butyl group.

1. Introduction

Room temperature ionic liquids (RTILs) are well-known to have some outstanding properties as solvents; for example, extremely low volatility and flammability, characteristic solubility, and wide electric windows. Hence, RTILs have attracted much attention as green solvents.[1−5] It is critically important to reveal the structures of RTILs in both the crystalline and liquid states for understanding their physicochemical properties. A number of reports have been made on the relationship between the properties and structures of constituent ions.[6−13] For example, the properties of imidazolium-based RTILs, such as melting point, viscosity, and density, clearly depend on the chain length of alkyl groups in imidazolium-based cations.[6,13] Recently, conformational variation of ions has also been understood to play an important role in determining the properties of RTILs.[9,14−21]

1-Butyl-3-methylimidazolium hexafluorophosphate ($[C_4mim]PF_6$) is one of the most typical RTILs because it consists of the representative cation and anion for RTILs. The chemical structure is shown in part a of Figure 1. There are some reports on the liquid[22−24] and crystalline[25,26] structures for $[C_4mim]PF_6$. For the crystal structure, two groups independently obtained crystals belonging to the same crystalline phase and reported that the butyl group of the cation is in gauche'−trans (*G'T*) conformation (part b of Figure 1).[25,26] From thermodynamic studies, some groups indicated that $[C_4mim]PF_6$ has two crystal polymorphs[25,27−31] and complex phase-transition behaviors.[25,29,31] For example, Choudhury et al.[25] and Troncoso et al.[31] reported a complicated melting curve from their DSC measurements. However, the crystalline structure and phase behaviors are not understood in detail.

In this study, the phase-transition behaviors and cation structures of $[C_4mim]PF_6$ were investigated by calorimetry and Raman spectroscopy equipped with a precise temperature-control stage. Consequently, we have found that $[C_4mim]PF_6$ has three crystal polymorphs, and all of the phase transitions except the glass transition occur accompanied by conformational changes of the butyl group around the C7−C8 axis.

2. Experimental Section

$[C_4mim]PF_6$ was prepared by metathesis of 1-butyl-3-methylimidazolium chloride with sodium hexafluorophosphate. The ionic liquid was purified by washing with distilled water and using activated charcoal, and characterized by ^{1}H NMR (JEOL JNM-LA500) and elemental analysis (Perkin-Elmer 2400). ^{1}H NMR (DMSO-d_6, δ/ppm relative to TMS) results were: 9.02 (s, 1H), 7.68 (s, 1H), 7.61 (s, 1H), 4.10 (t, 2H), 3.79 (s, 3H), 1.71 (m, 2H), 1.21 (m, 2H), 0.84 (t, 3H). Elemental analysis for $C_8H_{15}F_6N_2P$ calcd. (found) showed: C 33.81 (33.77), H 5.32 (4.96), N 9.86 (9.81). No chlorine ions could be detected on adding aqueous $AgNO_3$ solution to the RTIL. The RTIL was dried under vacuum of about 10^{-3} Pa at 313 K for one day before use. It was handled in an N_2 atmosphere glovebox to avoid absorption of atmospheric moisture. The water content of the RTILs after the complete preparation was about 140 ppm, as measured by Karl Fischer titration using a Mettler-Toledo model DL39 coulometer. We previously constructed an apparatus combining a commercially available Raman spectrometer and a laboratory-made calorimeter.[32] This is applicable as a Raman spectrometer equipped with a temperature controller with high stability (±0.001 K) as well as an apparatus for simultaneous measurement of vibrational spectroscopy and calorimetry. A Raman spectrometer with an optical fiber (HoloLab 5000, Kaiser Optical Systems) equipped with a GaAlAs diode laser (wavelength 785 nm) was used. A spectrum in the range of 100−3450 cm^{-1} can be measured at the same time with a spectral resolution of 4 cm^{-1} by adopting a multiplex grating backed up by a CCD camera. The maximum laser output power was 400 mW, and the laser spot diameter was ca. 80 μm. The laboratory-made calorimeter used here is a simpler type of our supersensitive DSC, the fundamental and original idea for which was previously reported.[33] These apparatuses use thermo modules as both a heat flow sensor and heat pumps,

* To whom correspondence should be addressed. Phone: +81-43-290-3939. Fax:+81-43-290-3939. E-mail: k.nishikawa@faculty.chiba-u.jp.
[†] Graduate School of Advanced Integration Science.
[‡] Faculty of Education.

10.1021/jp909256j
Published on Web 12/01/2009

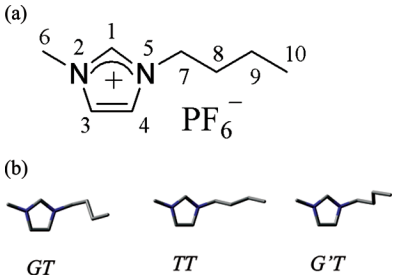

Figure 1. (a) Chemical structure of $[C_4mim]PF_6$ and numbering of atoms. (b) Gauche−trans (*GT*), trans−trans (*TT*), and gauche'−trans (*G'T*) conformations of $[C_4mim]^+$. Hydrogen atoms are omitted for simplicity.

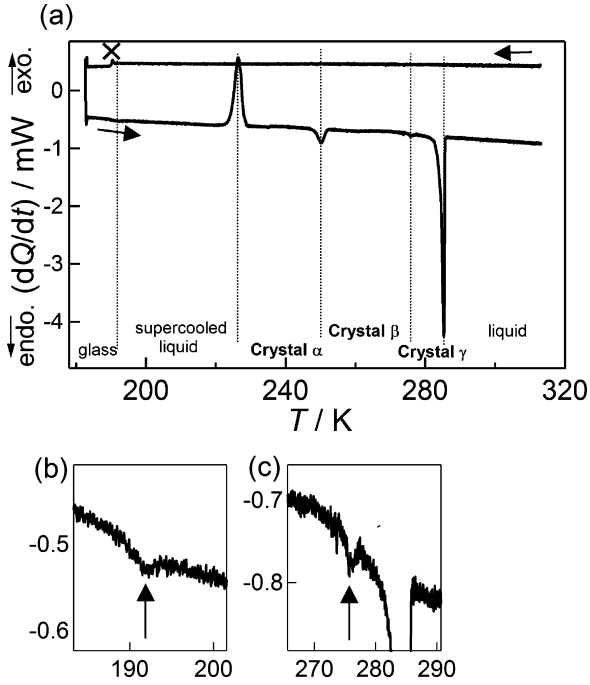

Figure 2. (a) Calorimetric curves of $[C_4mim]PF_6$ at a scanning rate of 5 mK/s for the whole temperature range. Expanded curves (b) around the glass transition and (c) around the phase transition from crystal β to crystal γ. The small peak observed at 190 K in the cooling process is an experimental artifact.

enabling us to perform calorimetric measurements with high sensitivity and high temperature stability. The baseline stability and temperature of the present calorimeter are measured to be ca. 5 μW and ±0.001 K, respectively. Temperature can be scanned at very slow heating and cooling rates (minimum value, 0.5 mK/s). Density functional theory (DFT) calculations were carried out using the *Gaussian 03* program package.[34] Both full geometry optimizations and normal frequency analyses for $[C_4mim]^+$ were performed for the gas phase using 6-311+G(d, p) basis sets according to Becke's three-parameter hybrid method[35] with the LYP correlation (B3LYP).[36,37] All optimized structures were found to produce no imaginary frequencies, which ensured the presence of a minimum. A scaling factor was applied to neither the calculated frequency nor thermal properties in this calculation.

3. Results and Discussion

3.1. Phase Transitions. Figure 2 shows calorimetric curves of $[C_4mim]PF_6$ in the range of 183−313 K. To follow and match the relatively slow thermodynamic changes of RTILs,[12,19,20,32,38,39] the measurements were performed at a scanning rate of 5 mK/s, which was much lower than the rates in typical calorimetric measurements. In the cooling process, no phase-transition peak appeared except for experimental artifact noise. On the other hand, several phase-transition peaks were observed in the heating process, such as the glass transition (192 K, part b of Figure 2), crystallization (226.5 K), two crystal−crystal transitions (250.3 K, 276 K), and melting (285.3 K). The temperature values in parentheses are peak-top values. The temperature for the present glass transition during heating is in good agreement with that obtained by adiabatic calorimetry, 190.6 K.[27] Although the transition from supercooled liquid to glass should occur during the cooling process, the signal could not be detected. This might be because the glass transition in the cooling process accidentally overlaps with the experimental artifact noise at about 190 K. Here, we call the three observed crystalline phases crystal α, crystal β, and crystal γ in order of increasing temperature.

TABLE 1: Melting Points (T_m) and Fusion Enthalpies (ΔH_{fusion}) of $[C_4mim]PF_6$

	this work	ref 10	ref 30	ref 27	ref 31	ref 28
T_m/K	284.3 (285.3)[a]	281	276.43	283.51	280.03	282
ΔH_{fusion}/kJ mol^{-1}	13.3	13.2	9.21	19.60	19.91	12

[a] This value is obtained when the peak-top is defined as the melting point.

First, the melting point (T_m) and fusion enthalpy (ΔH_{fusion}) obtained here are compared with previous reported values. The results are summarized in Table 1. We defined the peak-top of a melting curve for an RTIL as the melting temperature because RTILs usually melt accompanied by a premelting phenomenon.[12,19,20,32] Here, the value of the cross-point of the baseline and the rising curve of melting is tabulated in Table 1 for comparison with other reports. The peak-top value is written in parentheses. Prior to comparison of the values, we state that the purity of our sample is high enough to pass ^{1}H NMR, elemental analysis, Karl Fischer (water content is ca. 140 ppm), and $AgNO_3$ tests. Our T_m value is the highest of those reported. This finding can support the claim that our sample was pure enough to warrant discussion of its thermodynamic properties. Whereas the ΔH_{fusion} obtained here is comparable to the values reported by Fox et al.[10] and Jin et al.,[28] it is much lower than the values of Kabo et al.[27] and Troncoso et al.[31] The difference in ΔH_{fusion} may be attributed to the purity of the sample or differences in experimental methods or the process of data analysis. For example, Kabo et al. obtained their data with adiabatic calorimetry and did not mention the crystal−crystal phase transitions. Therefore, their values might be the enthalpy change including all of the phase transitions. Moreover, other possible reasons can be given based on the different thermal histories of the samples. As mentioned later, phase transitions accompany conformational changes of the cation, and therefore the state and structure of $[C_4mim]PF_6$ always depend on the thermal history.

Second, we focus on the crystal−crystal phase transitions. As mentioned above, we found two endothermic peaks at 250.3 and 276 K in our calorimetric curve between the crystallization and melting peaks. Most other groups detected only the signal corresponding to our larger peak at 250.3 K, and they reported that $[C_4mim]PF_6$ had two crystalline phases.[25,30] We think that the peak at 276 K is difficult to detect by DSC measurements with typical scanning rates because it is a very small peak that appears close to the melting peak, and the phase change seems to occur very slowly. Only Choudhury et al.[25] and Troncoso et al.[31] observed an endothermic peak besides the melting peak

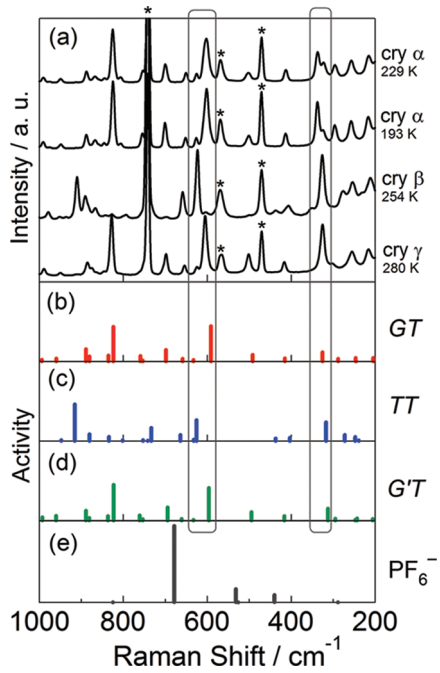

Figure 3. (a) Observed Raman spectra for the three crystalline phases. (b)−(e) Raman active bands calculated with DFT for the *GT*, *TT*, and *G'T* conformations of the cation and PF_6^-, respectively. Asterisks indicate the anion bands.

during melting but they gave no detailed discussion of the peak. Although their peak intensities differ from ours, we suppose that their peaks correspond to our small signal because the peak-top temperatures are similar. Although the signal at 276 K is very small, we can clearly distinguish two phases under our experimental conditions, and the two phases have different structures, as shown in the next section. We name the two phases crystal β and crystal γ. Thus, we have found three crystal phases for $[C_4mim]PF_6$ during the heating process.

3.2. Cation Structure in Each Phase. The structure of the $[C_4mim]^+$ ion in each crystalline phase was studied by Raman spectroscopy. The results are shown in part a of Figure 3. Raman bands in the range of 580−640 cm^{-1} are known as marker bands for rotational isomers of the butyl group in the $[C_4mim]^+$ ion.[14,40] The existence of nine rotational isomers of $[C_4mim]^+$ was demonstrated by quantum chemical calculations.[41,42] Taking into account both energy differences among the isomers[41,42] and results from single crystal structure analyses for $[C_4mim]^+$ salts,[9,21,25,26,43,44] we can pick three rotational isomers as possible conformers for $[C_4mim]^+$ in the crystal or liquid states, that is, the gauche−trans (*GT*), trans−trans (*TT*), and gauche'−trans (*G'T*) conformations caused by the rotation of the butyl group around the C7−C8 axis. The three isomers are shown in part b of Figure 1, and the corresponding active Raman bands from DFT calculations are displayed in parts b−d of Figure 3.

Crystal β has a distinguishable band at 624 cm^{-1}, which can be assigned to the *TT* (part c of Figure 3) conformation of $[C_4mim]^+$.[14] In the region of 580−640 cm^{-1}, the Raman spectrum of crystal α is similar to that of crystal γ. They have characteristic peaks at about 500, 600, and 700 cm^{-1}, suggesting that the cation structures in these crystalline phases will be assigned to the *GT* (part b of Figure 3)[14] or *G'T* (part d of Figure 3) conformations. The difference between crystal α and crystal γ is found in the region of 300−350 cm^{-1}. From the DFT calculations for $[C_4mim]^+$, the Raman bands observed at higher frequency (338 cm^{-1}) and lower frequency (326 cm^{-1}) are

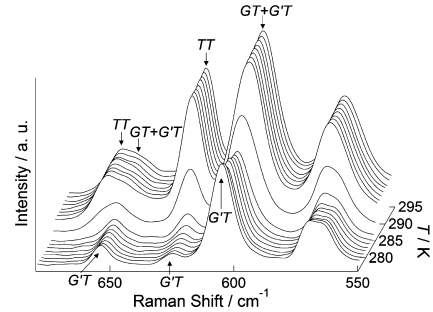

Figure 4. Temperature dependence of Raman spectra near the melting point. The scanning rate was 5 mK/s, and each spectrum was obtained every 1 K.

attributed to the *GT* and *G'T* conformations, respectively. As a result, crystal α can be assigned to *GT* and crystal γ to *G'T*.

It should be noted that a small component due to *G'T* conformation exists in crystal α. We studied the temperature dependence of the Raman scattering intensities of crystal α. The upper spectrum in part a of Figure 3 was measured at 229 K after crystallization during heating. The second spectrum was obtained from crystal α at 193 K during cooling. As expected, no phase transition occurred in the cooling process. If *GT* and *G'T* conformers coexist in an asymmetric unit in crystal α, as in the crystal of $[C_4mim]Tf_2N$,[21] the intensity ratio of the bands of higher (338 cm^{-1}) and lower (326 cm^{-1}) frequencies will not change. However, the band intensity at 326 cm^{-1} originating from *G'T* clearly decreases with falling temperature. This indicates that the most stable conformer in crystal α is *GT*, and we conclude that the conformation of the cation in crystal α is *GT*. We consider two possibilities for the origin of the appearance of *G'T*: 1) The rotational isomerism reaction between *GT* and *G'T* easily occurs in crystal α (i.e., low activation energy for rotational isomerism). 2) Part of the *G'T* conformer was left as amorphous solid or liquid without crystallization. We often observe the coexistence of crystals and supercooled liquid in RTILs.

The $[C_4mim]^+$ ion in the $[C_4mim]PF_6$ crystalline phase was reported to take the *G'T* conformation from single-crystal structure analyses at 173[26] and 193 K.[25] These results seem to be inconsistent with our finding because the *G'T* conformer appears in crystal γ, which is the highest-temperature crystalline phase. However, this apparent inconsistency can be resolved by the complex thermal history of $[C_4mim]PF_6$.[29] Moreover, we measured Raman spectra of crystal γ at 193 K (not shown), which were obtained by cooling from crystal γ with no phase transition. The two groups grew single crystals by different methods.[25,26] We suppose that the crystals they first made were crystal γ, and their structures were kept down to the measurement temperatures without a phase transition.

Figure 4 shows the temperature dependence of Raman spectra during melting. This region includes the phase transition from crystal γ (*G'T*) to liquid. The band at 624 cm^{-1} that is assigned to the *TT* conformation arises through melting, and behaviors such as the appearance or disappearance of bands characteristic to each conformation were observed in other phase-transition regions. Therefore, we can conclude that all phase transitions of $[C_4mim]PF_6$ except the glass transition accompany conformational change of the butyl group. It is noted that structural change in the cation occurs abruptly just near the peak-top temperature of melting, although the premelting phenomenon starts at a temperature 4−5 K lower. The same tendencies were observed in the melting processes of $[C_4mim]Br$[32] and $[i\text{-}C_3mim]Br$.[19] In our reported results on RTILs,[19,20,32] the

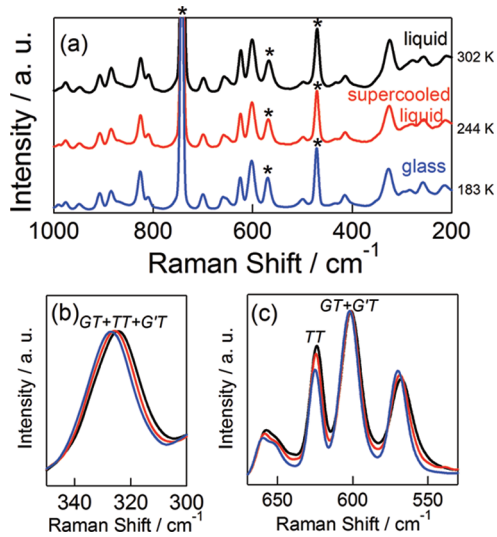

Figure 5. Raman spectra at liquid (302 K), supercooled (244 K), and glass states (183 K) in the range of (a) 200−1000 cm^{-1}, (b) 300−350 cm^{-1}, and (c) 530−670 cm^{-1}. Asterisks indicate the anion bands.

TABLE 2: Cation Conformations in Crystal Structure of [C_4mim]X Obtained by X-ray Diffraction

anion	Cl[9,43]	Br[9]	I[44]	Tf_2N[21]	CH_3SO_3[45]	CH_3SO_4[45]	PF_6[25,26]
conformation	*TT,GT*	*GT*	*GT*	*GT+G'T*	*GT*	*GT*	*G'T*

conformational changes of constituent ions seem to be delayed after the start of the thermal sign of the phase transitions.

Part a of Figure 5 shows the Raman spectra of [C_4mim]PF_6 in the liquid (at 302 K), supercooled liquid (at 244 K in the cooling process), and glass (at 183 K) states. These spectra resemble each other, which shows that the three states are composed of cations with similar structure. According to the Raman spectra in the range of 300−350 cm^{-1} (part b of Figure 5) and 530−670 cm^{-1} (part c of Figure 5), the *GT*, *TT*, and *G'T* conformers are considered to be mixed in those states, as in other imidazolium-based ionic liquids.[14,15,19,40]

Many crystal structures have been reported for the [C_4mim]$^+$ salts.[9,21,25,26,43−45] Some typical results are summarized in Table 2. The cation conformations in these crystal structures are concentrated on the *GT* conformation. Our Raman scattering study shows the existence of three types of crystalline phase for [C_4mim]PF_6, where conformations of the cation differ. To the best of our knowledge, no report has been made on [C_4mim]-based RTILs with *GT*, *TT*, and *G'T* in their crystals. [C_4mim]PF_6 will be one of the most representative examples showing the conformational variety of RTILs. At the same time, the complex isomerization of the constituent cations has caused some confusion regarding the phase behaviors and thermodynamic properties of [C_4mim]PF_6.

3.3. Enthalpy Difference. Enthalpy differences among the conformations can be obtained by comparing the intensities of Raman bands at different temperatures.[15,19,46] If enthalpy difference trends are similar for the liquid, supercooled liquid, and glass states, the differences can be estimated from the results shown in Figure 5. Parts b and c of Figure 5 compare the Raman spectra in the ranges of 300−350 cm^{-1} and 530−670 cm^{-1}, respectively. Only one peak is observed in the 300−350 cm^{-1} range (part b of Figure 5), and it shifts slightly to lower frequency with increasing temperature. This peak overlaps the bands of the *GT*, *TT*, and *G'T* conformations, and the *GT* band is observed at higher frequency (Figure 3). This finding indicates that the contribution of the *GT* conformer is larger at lower temperature and thus has lower energy than the average of the *TT* and *G'T* conformations. As shown in part c of Figure 5, the Raman band intensity at 624 cm^{-1} attributed to the *TT* conformation increases with increasing temperature. This shows that the average energy of the *GT* and *G'T* conformations is lower than that of the *TT* conformation. These findings suggest an enthalpy order of $GT < TT \approx G'T$ in these states. This result is consistent with the appearance of the crystalline phases ($GT < TT \leq G'T$).

TABLE 3: Phase-Transition Temperatures (T_{trans}), Phase-Transition Enthalpies (ΔH_{trans}), and Cation Conformations for Each Phase

	supercooled liquid	crystal α	crystal β	crystal γ	liquid
T_{trans}[a]/K		226.5	250.3	276.1	285.3
ΔH_{trans}[b] /kJ mol^{-1}		0	1.7	1.9	
conformation	*mixture*	*GT*	*TT*	*G'T*	*mixture*

[a] T_{trans} is defined by the peak-top of the calorimetric curve. [b] Difference from crystal α.

The phase-transition point (T_{trans}), phase-transition enthalpy (ΔH_{trans}), and cation conformation for each phase are summarized in Table 3. The enthalpy differences among the three conformers estimated from DFT calculation ($\Delta H^{cal}_{conformation}$) are −2.4 kJ mol^{-1} for *TT* and −1.8 kJ mol^{-1} for *G'T* from the enthalpy energy for *GT*. The agreement between ΔH_{trans} and $\Delta H^{cal}_{conformation}$ is not good in this study. This is because $\Delta H^{cal}_{conformation}$ does not include the anion contribution. However, the range of ΔH_{trans} (ca. 2 kJ mol^{-1}) corresponds to that of $\Delta H^{cal}_{conformation}$.

It is difficult to explain why three crystalline phases linked with conformational changes of the butyl group appear only in [C_4mim]PF_6. One possible reason is that interionic interaction is relatively weak because of the large anion size of PF_6^- and the delocalization of the negative charge. More detailed structural and thermodynamic data will be required to reveal the origin of the three crystalline phases in [C_4mim]PF_6.

4. Conclusions

We have investigated the thermodynamic behaviors and related conformational structures of [C_4mim]PF_6 with calorimetry and Raman spectroscopy. Although [C_4mim]PF_6 is regarded as one of the most typical RTILs, the thermodynamic properties and conformations of the cation have been unclear due to its complex phase-transition behaviors. In this article, three crystalline phases have been discovered in [C_4mim]PF_6 by calorimetric measurement at a very slow scanning rate (5 mK/s). The cation conformations of these phases were identified as *GT*, *TT*, and *G'T* in order of increasing enthalpy. A similar trend was also obtained among the liquid, supercooled liquid, and glass states based on analysis of the temperature dependences of intensities for the Raman bands characteristic of the conformations. However, the order of enthalpy did not agree with the results obtained by DFT calculations for free [C_4mim]$^+$ ions. [C_4mim]PF_6 is the first sample where three types of rotational conformer for the butyl group appear in the crystalline phases individually. Also, it is a good example to demonstrate that conformational variety is an important factor in determining the thermodynamic properties of RTILs.

Acknowledgment. The present study was supported in part by the Ministry of Education, Culture, Sports, Science and Technology (MEXT) of Japan (No. 17073002, Grant-in-Aids

for Scientific Research in Priority Area "Science of Ionic Liquids" (K. N.); No. 21245003, Grant-in-Aids for Scientific Research (A) (K. N.)). This work was also partially supported by Chiba University (Research Support Program for Young Scientists (A) and the Global Center-of-Excellence Program "Advanced School for Organic Electronics" supported by MEXT (T. E.)).

References and Notes

(1) *Ionic Liquids in Syntheses*; Wasserscheid, P., Welton, T., Eds.; VCH-Wiley: Weinheim, Germany, 2003.

(2) *Electrochemical Aspects of Ionic Liquids*; Ohno, H., Ed.; Wiley-Interscience: Hoboken, NJ, 2005.

(3) Welton, T. *Chem. Rev.* **1999**, *99*, 2071–2083.

(4) Wasserscheid, P.; Keim, W. *Angew. Chem., Int. Ed.* **2000**, *39*, 3772–3789.

(5) Sheldon, K. R. *Chem. Commun.* **2001**, 2399–2407.

(6) Holbrey, J. D.; Seddon, K. R. *J. Chem. Soc., Dalton Trans.* **1999**, 2133–2139.

(7) Ngo, H. L.; LeCompte, K.; Hargens, L.; McEwen, A. B. *Thermochim. Acta* **2000**, *357*−*358*, 97–102.

(8) Dzyuba, S. V.; Bartsch, R. A. *ChemPhysChem* **2002**, *3*, 161–166.

(9) Holbrey, J. D.; Reichert, W. M.; Nieuwenhuyzen, M.; Johnston, S.; Seddon, K. R.; Rogers, R. D. *Chem. Commun.* **2003**, 1636–1637.

(10) Fox, D. M.; Awad, W. H.; Gilman, J. W.; Maupin, P. H.; De Long, H. C.; Trulove, P. C. *Green Chem.* **2003**, *5*, 724–727.

(11) Paulechka, Y. U.; Kabo, G. J.; Blokhin, A. V.; Shaplov, A. S.; Lozinskaya, E. I.; Vygodskii, Y. S. *J. Chem. Thermodyn.* **2007**, *39*, 158–166.

(12) Nishikawa, K.; Wang, S.; Katayanagi, H.; Hayashi, S.; Hamaguchi, H.; Koga, Y.; Tozaki, K. *J. Phys. Chem. B* **2007**, *111*, 4894–4900.

(13) Huddleston, J. G.; Visser, A. E.; Reichert, W. M.; Willauer, H. D.; Broker, G. A.; Rogers, R. D. *Green Chem.* **2001**, *3*, 156–164.

(14) Ozawa, R.; Hayashi, S.; Saha, S.; Kobayashi, A.; Hamaguchi, H. *Chem. Lett.* **2003**, *32*, 948–949.

(15) Umebayashi, Y.; Fujimori, T.; Sukizaki, T.; Asada, M.; Fujii, K.; Kanzaki, R.; Ishiguro, S. *J. Phys. Chem. A* **2005**, *109*, 8976–8982.

(16) Berg, R. W.; Deetlefs, M.; Seddon, K. R.; Shim, I.; Thompson, J. M. *J. Phys. Chem. B* **2005**, *109*, 19018–19025.

(17) Fujii, K.; Fujimori, T.; Takamuku, T.; Kanzaki, R.; Umebayashi, Y.; Ishiguro, S. *J. Phys. Chem. B* **2006**, *110*, 8179–8183.

(18) Berg, R. W. *Mon. Chem.* **2007**, *138*, 1045–1075.

(19) Endo, T.; Nishikawa, K. *J. Phys. Chem. A* **2008**, *112*, 7543–7550.

(20) Nishikawa, K.; Wang, S.; Endo, T.; Tozaki, K. *Bull. Chem. Soc. Jpn.* **2009**, *82*, 806–812.

(21) Paulechka, Y. U.; Kabo, G. J.; Blokhin, A. V.; Shaplov, A. S.; Lozinskaya, E. I.; Golovanov, D. G.; Lyssenko, K. A.; Korlyukov, A. A.; Vygodskii, Y. S. *J. Phys. Chem. B* **2009**, *113*, 9538–9546.

(22) Morrow, T. I.; Maginn, E. J. *J. Phys. Chem. B* **2002**, *106*, 12807–12813.

(23) Antony, J. H.; Mertens, D.; Breitenstein, T.; Dölle, A.; Wasserscheid, P.; Carper, W. R. *Pure Appl. Chem.* **2004**, *76*, 255–261.

(24) Urahata, S. M.; Ribeiro, M. C. C. *J. Chem. Phys.* **2005**, *122*, 024511–9.

(25) Choudhury, A. R.; Winterton, N.; Steiner, A.; Cooper, A. I.; Johnson, K. A. *J. Am. Chem. Soc.* **2005**, *127*, 16792–16793.

(26) Dibrov, S. M.; Kochi, J. K. *Acta Crystallogr.* **2006**, *C62*, o19–o21.

(27) Kabo, G. J.; Blokhin, A. V.; Paulechka, Y. U.; Kabo, A. G.; Shymanovich, M. P.; Magee, J. W. *J. Chem. Eng. Data* **2004**, *49*, 453–461.

(28) Jin, H.; O'Hare, B.; Dong, J.; Arzhantsev, S.; Baker, G. A.; Wishart, J. F.; Benesi, A. J.; Maroncelli, M. *J. Phys. Chem. B* **2008**, *112*, 81–92.

(29) Triolo, A.; Mandanici, A.; Russina, O.; Rodriguez-Mora, V.; Cutroni, M.; Hardacre, C.; Nieuwenhuyzen, M.; Bleif, H.-J.; Keller, L.; Ramos, M. A. *J. Phys. Chem. B* **2006**, *110*, 21357–21364.

(30) Domańska, U.; Marciniak, A. *J. Chem. Eng. Data* **2003**, *48*, 451–456.

(31) Troncoso, J.; Cerdeiriña, C. A.; Sanmamed, Y. A.; Romaní, L.; Rebelo, L. P. N. *J. Chem. Eng. Data* **2006**, *51*, 1856–1859.

(32) Endo, T.; Tozaki, K.; Masaki, T.; Nishikawa, K. *Jpn. J. Appl. Phys.* **2008**, *47*, 1775–1779.

(33) Wang, S.; Tozaki, K.; Hayashi, H.; Inaba, H. *J. Therm. Anal. Calorim.* **2005**, *79*, 605–613.

(34) Frisch, M. J.; Trucks, G. W.; Schlegel, H. B.; Scuseria, G. E.; Robb, M. A.; Cheeseman, J. R.; Montgomery, J. A., Jr.; Vreven, T.; Kudin, K. N.; Burant, J. C.; Millam, J. M.; Iyengar, S. S.; Tomasi, J.; Barone, V.; Mennucci, B.; Cossi, M.; Scalmani, G.; Rega, N.; Petersson, G. A.; Nakatsuji, H.; Hada, M.; Ehara, M.; Toyota, K.; Fukuda, R.; Hasegawa, J.; Ishida, M.; Nakajima, T.; Honda, Y.; Kitao, O.; Nakai, H.; Klene, M.; Li, X.; Knox, J. E.; Hratchian, H. P.; Cross, J. B.; Adamo, C.; Jaramillo, J.; Gomperts, R.; Stratmann, R. E.; Yazyev, O.; Austin, A. J.; Cammi, R.; Pomelli, C.; Ochterski, J. W.; Ayala, P. Y.; Morokuma, K.; Voth, G. A.; Salvador, P.; Dannenberg, J. J.; Zakrzewski, V. G.; Dapprich, S.; Daniels, A. D.; Strain, M. C.; Farkas, O.; Malick, D. K.; Rabuck, A. D.; Raghavachari, K.; Foresman, J. B.; Ortiz, J. V.; Cui, Q.; Baboul, A. G.; Clifford, S.; Cioslowski, J.; Stefanov, B. B.; Liu, G.; Liashenko, A.; Piskorz, P.; Komaromi, I.; Martin, R. L.; Fox, D. J.; Keith, T.; Al-Laham, M. A.; Peng, C. Y.; Nanayakkara, A.; Challacombe, M.; Gill, P. M. W.; Johnson, B.; Chen, W.; Wong, M. W.; Gonzalez, C.; Pople, J. A. *Gaussian 03*; 2004.

(35) Becke, A. D. *J. Chem. Phys.* **1993**, *98*, 5648–5652.

(36) Lee, C.; Yang, W.; Parr, R. G. *Phys. Rev. B* **1988**, *37*, 785–789.

(37) Miehlich, B.; Savin, A.; Stoll, H.; Preuss, H. *Chem. Phys. Lett.* **1989**, *157*, 200–206.

(38) Nishikawa, K.; Tozaki, K. *Chem. Phys. Lett.* **2008**, *463*, 369–372.

(39) Nishikawa, K.; Wang, S.; Tozaki, K. *Chem. Phys. Lett.* **2008**, *458*, 88–91.

(40) Hayashi, S.; Ozawa, R.; Hamaguchi, H. *Chem. Lett.* **2003**, *32*, 498–499.

(41) Turner, E. A.; Pye, C. C.; Singer, R. D. *J. Phys. Chem. A* **2003**, *107*, 2277–2288.

(42) Tsuzuki, S.; Arai, A. A.; Nishikawa, K. *J. Phys. Chem. B* **2008**, *112*, 7739–7747.

(43) Saha, S.; Hayashi, S.; Kobayashi, A.; Hamaguchi, H. *Chem. Lett.* **2003**, *32*, 740–741.

(44) Nakakoshi, M.; Shiro, M.; Fujimoto, T.; Machinami, T.; Seki, H.; Tashiro, M.; Nishikawa, K. *Chem. Lett.* **2006**, *35*, 1400–1401.

(45) Santos, C. S.; Rivera, R. S.; Dibrov, S.; Baldelli, S. *J. Phys. Chem. C* **2007**, *111*, 7682–7691.

(46) Lassegues, J. C.; Grondin, J.; Holomb, R.; Johansson, P. *J. Raman Spectrosc.* **2007**, *38*, 551–558.

JP909256J